Environmental Science and Pollution Research (2023) 30:4151–4165
https://doi.org/10.1007/s11356-022-22487-x

RESEARCH ARTICLE

$MoSe_2$-modified ZIF-8 novel nanocomposite for photocatalytic remediation of textile dye and antibiotic-contaminated wastewater

Honey Mittal[1] · Aruna Ivaturi[2] · Manika Khanuja[1]

Received: 3 March 2022 / Accepted: 7 August 2022 / Published online: 13 August 2022

Abstract

COVID-19-led antibiotic waste generated from hospitals and health centres may cause serious health issues and significantly impact the environment. In the coming decades, antibiotic resistance will be one of the most significant threats to global human health. Photocatalytic water remediation is an effective and promising environmental solution that can be utilized to address this issue, to convert antibiotic waste into non-toxic products by utilizing renewable and abundant solar energy. In the present study, a novel nanocomposite of zeolitic imidazolate frameworks (ZIF-8) and molybdenum diselenide ($MoSe_2$) was efficiently synthesized by the solvothermal method for the complete degradation of the antibiotics and textile waste from water. The morphology, crystallinity and band gap of the samples were characterized by field emission scanning electron microscopy (FESEM), X-ray diffraction (XRD) and UV–visible spectroscopy. Fourier transform infrared spectroscopy (FTIR) and X-ray photoelectron spectroscopy (XPS) provide the binding information of the sample. The photocatalytic activity was tested for degradation of the antibiotics (tetracycline hydrochloride (TC) and metronidazole (MNZ)) used in COVID-19 treatment and textile dye (malachite green). Time-resolved photoluminescence spectroscopy confirmed the enhanced charge separation in the $MoSe_2$@ZIF-8 nanocomposite with an average lifetime of 4.72 ns as compared to pristine samples. The nanocomposite showed ~ 100% removal efficiency with rate constants of 63×10^{-3}, 49×10^{-3} and 42×10^{-3} min^{-1} for TC, MNZ and malachite green, respectively. The photocatalytic degradation of TC was carried out under different pH conditions (4, 7 and 9), and the degradation mechanism was explained on the basis of zeta potential measurements and active species trapping experiment. The by-products of the photocatalytic treatment of TC antibiotics were tested using liquid chromatography-mass spectroscopy (LC–MS), and they were found to be non-toxic for aquatic and human life. The regeneration property of the nanocomposite was confirmed by FESEM with regeneration efficiency of 88.7% in the 4th cycle. Thus, $MoSe_2$@ZIF-8-based photocatalysts have potential application in water remediation, especially in making the antibiotic waste less toxic.

Keywords TCSPC · Photocatalysis · Zeta potential · Antibiotics · COVID-19

Introduction

COVID-19 has resulted in an increased pharmaceutical waste in the environment, rivers and coastal waters (Chen et al. 2021) (Dharmaraj et al. 2021). Antibiotic waste management is a critical problem because of its high environmental and human health hazards (Tsai 2021; Wang et al. 2020a). Antibiotics are not easily metabolized resulting in the expulsion of their residues through faeces and urine to the aquatic ecosystem leading to serious environmental problems (Li et al. 2020). Moreover, these antibiotics cannot be removed by traditional procedures such as biological processes, filtration, coagulation and sedimentation (Adams et al. 2002; Barhoumi et al. 2017; Stackelberg et al. 2007).

Responsible Editor: Sami Rtimi

✉ Manika Khanuja
manikakhanuja@gmail.com

[1] Centre for Nanoscience and Nanotechnology, Jamia Millia Islamia, New Delhi 110025, India

[2] Smart Materials Research and Device Technology (SMaRDT) Group, Department of Pure and Applied Chemistry, University of Strathclyde, Glasgow G1 1XL, UK

Tetracycline hydrochloric (TC) antibiotics and metronidazole (MNZ) have been explored as potential therapeutic drugs in treating COVID-19 patients because of their potential antiviral properties (Gharebaghi et al. 2020, Sodhi and Etminan 2020). Tetracycline hydrochloric antibiotics are primary antibiotic groups found in the different ecosystems that are used for human therapy (viral infections and inflammatory disorders) and agricultural purposes (Daghrir and Drogui 2013; Sodhi and Etminan 2020). Recently, a computational study has shown that TC plays a key role in treating SARS-CoV-2 main proteases and COVID-19-related lung disease (Gironi et al. 2020). Metronidazole (MNZ) is the most widely used second-generation quinolones and is used to treat joint infections, gastroenteritis, respiratory tract infections and cellulitis. MNZ is a redox-active prodrug that acts as a biocidal agent, and studies have revealed that it decreases the COVID-19 infection (Gharebaghi et al. 2020). However, MNZ induces an acute and sub-lethal effect on most species of aquatic life. One serious water pollution concern involving the discharge of antibiotic waste into the water bodies is the possibility of the development of antibiotic-resistant bacteria in the wastewater (Dharmaraj et al. 2021). Dyes are primary constituents of textile wastewater and constitute a group of toxic and carcinogenic contaminants.

For the treatment of antibiotic and textile wastewater, photocatalysis is a facile, highly efficient environment-friendly and straightforward technology as compared to other conventional techniques (Adams et al. 2002; Ashraf et al. 2020; Kumar et al. 2022, 2020; Mittal et al. 2019; Qin et al. 2021). ZIF-8 has been considered a potential photocatalyst for CO_2 reduction, water splitting and photocatalytic degradation due to its large surface areas, well-defined porous structures and superior photocatalytic performance (Chin et al. 2018; Li et al. 2019b; Peng et al. 2020; Shinde et al. 2021). However, ZIF-8-based photocatalysts are limited due to the low electron discharge ability and high recombination rate of photogenerated electron–hole pairs (Fu and Ren 2020; Qiu et al. 2018). Therefore, to overcome the issues related to ZIF-8 and improve its catalytic performance, the nanocomposite of ZIF-8 with $MoSe_2$ was constructed. Molybdenum diselenide ($MoSe_2$) has been proven to be a potential co-catalyst for photocatalysis due to more active sites and reduced recombination rate of charge carriers (Mittal and Khanuja 2020a; Siddiqui et al. 2018). Therefore, it is advantageous to construct a nanocomposite by combining the photocatalytic properties of $MoSe_2$ with the strong adsorbing properties of ZIF-8 to generate a potential photocatalyst to degrade antibiotic wastes.

In this study, we have synthesized a novel photocatalyst by a two-step method: the hydrothermal method for $MoSe_2$ and the solvothermal method for the synthesis of the $MoSe_2$@ZIF-8 nanocomposite. A series of pollutants (antibiotics: TC, MNZ and dye: malachite green) are used to evaluate the degradation efficiency of the synthesized samples. The $MoSe_2$@ZIF-8 nanocomposite showed enhanced degradation efficiency, ~ 3 times higher than pristine $MoSe_2$. The degradation efficiency obtained at different pH (4, 7 and 9) was explained using zeta potential measurements. The highest degradation efficiency for TC was observed in the alkaline medium due to the effect of electrostatic attraction between TC^{2-} and the positive charge on the surface of the nanocomposite. The proposed photocatalysis mechanism was supported by a scavenger experiment that confirms the role of active species in the degradation of pollutants. Repeated experiments confirmed the reusability and regeneration ability of the nanocomposite. To the best of our knowledge, the $MoSe_2$@ZIF-8 nanocomposite has not been reported before for wastewater treatment.

Experimental section

Materials

Sodium molybdate (Na_2MoO_4) with 99.99% purity and hydrochloric acid ($HCl{\cdot}H_2O$) with 99.96% purity were bought from Thermo Fisher Scientific India Pvt. Ltd. Selenium (Se, 99.99%) and hydrazine hydrate ($N_2H_4{\cdot}H_2O$) with 98% purity were bought from Central Drug House Pvt. Ltd. To prepare ZIF-8, 2-methylimidazole (98%) and zinc nitrate ($Zn(NO_3)_2$) were obtained from Loba Chemie Pvt. Ltd. Milli-Q water was used for all the experimental work.

Synthesis of $MoSe_2$@ZIF-8 nanocomposite

For the synthesis of ZIF-8, solution A was prepared by dissolving 0.585 g of zinc nitrate in 4 mL of Milli-Q water using a magnetic stirrer. Solution B was prepared by dissolving 2-methylimidazole in 40 mL of Milli-Q water also known as linker solution, followed by addition of 6 mL of DMSO. Solution A was then added to the linker solution and magnetically stirred for 5 min, forming a milky white solution. The obtained solution was centrifuged at 15,000 rpm for 15 min followed by washing and drying to yield ZIF-8 (Kaur et al. 2017). $MoSe_2$ was prepared by the hydrothermal method according to a previously reported study (Mittal and Khanuja 2020a). Figure 1 shows the schematic for the synthesis of the $MoSe_2$@ZIF-8 nanocomposite. The $MoSe_2$@ZIF-8 nanocomposite was synthesized using a similar method as ZIF-8. In the above procedure, 0.1 g of $MoSe_2$ was dissolved in 6 mL of DMSO before its addition to the linker solution and magnetically stirred for 5 min. All the further steps were similar to the synthesis of pristine ZIF-8

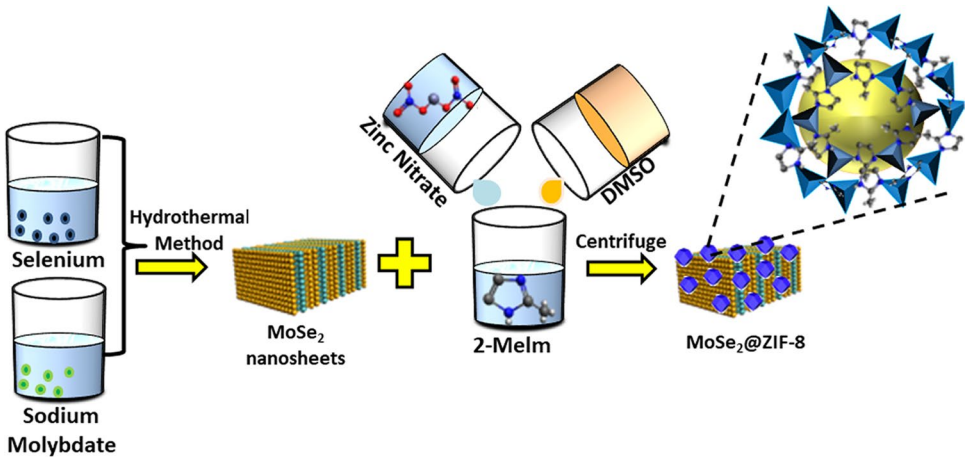

Fig. 1 Synthesis mechanism of $MoSe_2$@ZIF-8 nanocomposite

(Chen et al. 2019). Finally, obtained $MoSe_2$@ZIF-8 material was labelled as ZM.

Characterization

The morphology of the prepared samples was characterized using a FESEM-field emission scanning electron microscope (Quanta 3D FEG). X-ray diffraction (XRD) diffractograms were recorded using Rigaku SmartLab XRD. Samples were characterized for optical study using a UV–Vis spectrometer (Agilent Technologies, Cary 100 Series). Thin films of the samples were prepared by dissolving in ethanol for functional group study, and spectra were recorded by Fourier transform infrared (FTIR) spectroscopy (Bruker Tensor 37 FTIR spectrometer). X-ray photoelectron spectroscopy (XPS) was performed on ESCA + Omicron Nano Technology with a characteristic energy of 1486.7 eV. Surface charge measurement of the samples was performed using zeta potential (Malvern Zetasizer Nano ZS) using ethanol as dispersing solvent. Time-correlated single photon counting (TCSPC) measurement of the samples was recorded using a spectrometer (Horiba (DeltaFlex01-DD)). The intermediate and final degraded products of antibiotic degradation solution were examined by liquid chromatography-mass spectroscopy (LC–MS) from the Xevo TQD system.

Results and discussion

Morphology and components

Figure 2(a)–(c) shows FESEM micrographs of ZIF-8, $MoSe_2$ and ZM nanocomposites. It is observable in Fig. 2(a) that pure ZIF-8 nanoparticles are polyhedrons with an average particle size of ~ 300 nm. Figure 2(b) clearly shows the nanosheets of $MoSe_2$. As shown in Fig. 2(c), ZM nanocomposites consist of well-shaped polyhedrons of ZIF-8 nanoparticles with an average particle size of about 116 nm uniformly dispersed on the surface of $MoSe_2$ nanosheets.

The structural properties of $MoSe_2$, ZIF-8 and the ZM nanocomposite were investigated by XRD (Fig. 3(a)–(c)). The XRD pattern of the pristine ZIF-8 (Fig. 3(a)) showed diffraction peaks at 7.3°, 10.3°, 12.7°, 14.7°, 16.4°, 18.0°, 19.3°, 22.1°, 24.6°, 25.6°, 26.7°, 30.6° and 32.3° corresponding to (011), (002), (112), (022), (013), (222), (123), (114) (233), (224), (223), (044) and (235) planes of ZIF-8, respectively (JCPDS Card No: JCPDS 00–062-1030) (Si et al. 2018). In $MoSe_2$ (Fig. 3(b), the main peak at 29.6° corresponds to the (004) plane. Both ZIF-8 and $MoSe_2$ peaks were observed in the ZM nanocomposite, which implies that ZIF-8 is in close contact with the $MoSe_2$ nanosheets.

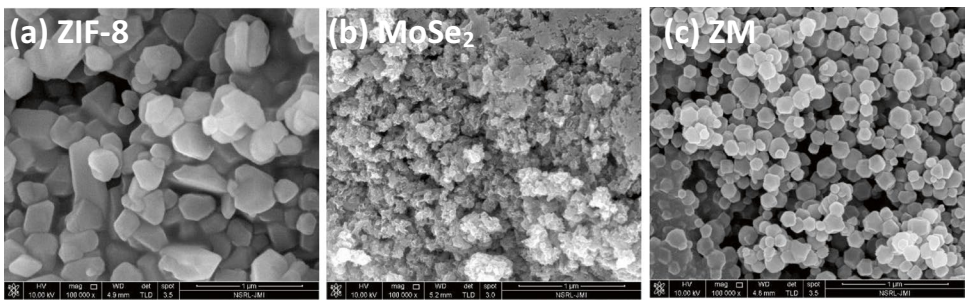

Fig. 2 FESEM images of (**a**) ZIF-8, (**b**) $MoSe_2$ and (**c**) ZM nanocomposite

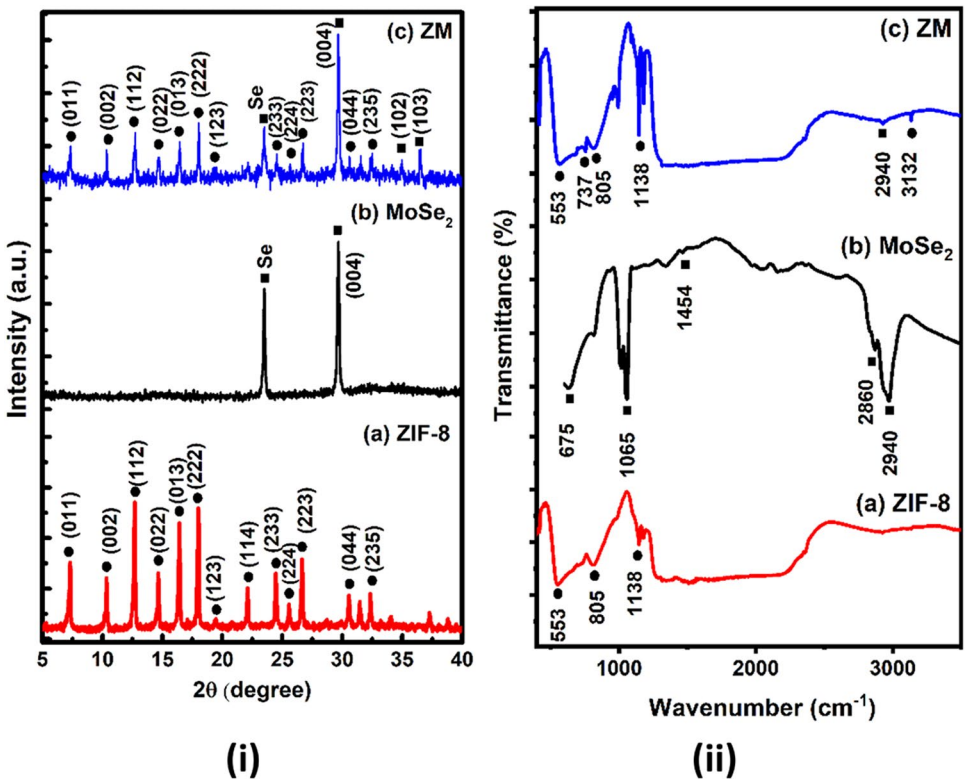

Fig. 3 (i) XRD diffractograms and (ii) FTIR spectra of (**a**) ZIF-8, (**b**) $MoSe_2$ and (**c**) ZM nanocomposite

FTIR spectra of ZIF-8, $MoSe_2$ and ZM nanocomposite are shown in Fig. 3 ii(a)–(c). ZIF-8 and ZM have similar FTIR peaks, indicating that surface modification does not destroy the fundamental structural framework. In the FTIR spectra of ZIF-8 as shown in Fig. 3 ii(a), the bands at 553 cm^{-1} and 805 cm^{-1} are assigned to the out-of-plane blending of 2-methyl imidazole rings (Ulu 2020). The peak located at 1138 cm^{-1} is assigned to the C–N vibration of the imidazole ring (Wu et al. 2017). In the FTIR spectra of $MoSe_2$ as shown in Fig. 3 ii(b), the peaks located at 1065 cm^{-1} and 1454 cm^{-1} are assigned to the Se–O and carboxylate (COO^-) stretch, respectively (Liu et al. 2017). The peaks located at higher frequencies 2860 cm^{-1} and 2940 cm^{-1} are attributed to the presence of acyclic stretching of C–H (Harpeness et al. 2003; Liu et al. 2017). Compared with the FTIR analysis of pristine ZIF-8, the ZM nanocomposite (Fig. 3 ii(c)) showed the existence of an adsorption band at 3132 cm^{-1} corresponding to the methyl group present in the linker and imidazole ring (Kaur et al. 2017).

UV–Vis absorption spectra of the ZIF-8, $MoSe_2$ and ZM nanocomposites are shown in Fig. 4i(a)–(c), respectively. All the samples show absorbance in the wavelength range of 200 to 800 nm. ZIF-8 had maximum absorbance at 305 and 350 nm, the ZM nanocomposite at 340 and 365 nm.

The band gap of samples is calculated from the Tauc plot as shown in Fig. 4 ii(a)–(c). The energy band gap values were calculated using Eq. (1):

$$\alpha h\nu = (h\nu - E_g)^n \tag{1}$$

where h is the Planck's constant, α is the absorption coefficient, ν is the frequency, E_g is the bandgap of the photocatalyst and n is the number that determines the transition property which is taken as 0.5 for the direct bandgap and 2 for the indirect bandgap semiconductor (Mittal and Khanuja 2021). In this case, $MoSe_2$ is an indirect bandgap semiconductor whereas ZIF-8 is a direct bandgap semiconductor; however, in the bandgap calculations of the ZM nanocomposite, n is taken as 0.5 because ZIF-8 is the base material (Chen et al. 2019). The $MoSe_2$, ZIF-8 and ZM nanocomposites exhibited absorbance in the visible region with the band gap of 1.71 eV, 2.70 eV and 3.22 eV, respectively.

XPS spectra were used to investigate the elemental valence and bonding information of the ZM nanocomposite. The survey spectrum shown in Fig. 5(a) confirms the presence of Zn, Mo, Se, C, O and N. The peaks located at 1021.6 eV and 1044.6 eV binding energies in Fig. 5(b) are assigned to Zn $2p_{3/2}$ and Zn $2p_{1/2}$ of Zn^{2+}, respectively (Jia et al. 2018). As seen in Fig. 5(c), peaks centred at 229.78 eV and 233.1 eV correspond to the binding energies of Mo(V)($3d_{5/2}$) and Mo(V)($3d_{3/2}$), respectively, which indicates the formation of Mo–Se bonds, whereas peaks at 228.27 and 231.54 eV correspond to Mo^{4+} characteristics and peaks at 231.72 and 235.03 eV correspond to Mo^{6+}, respectively. The XPS results of Se 3d are

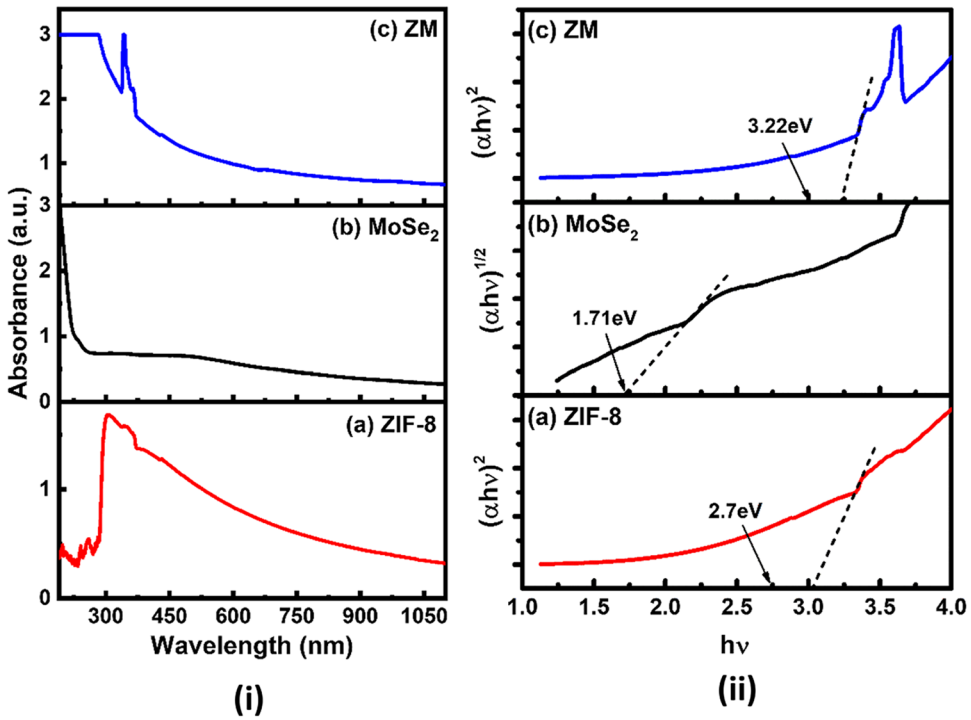

Fig. 4 (i) UV absorbance spectra and (ii) Tauc plot of (**a**) ZIF-8, (**b**) $MoSe_2$ and (**c**) ZM nanocomposite

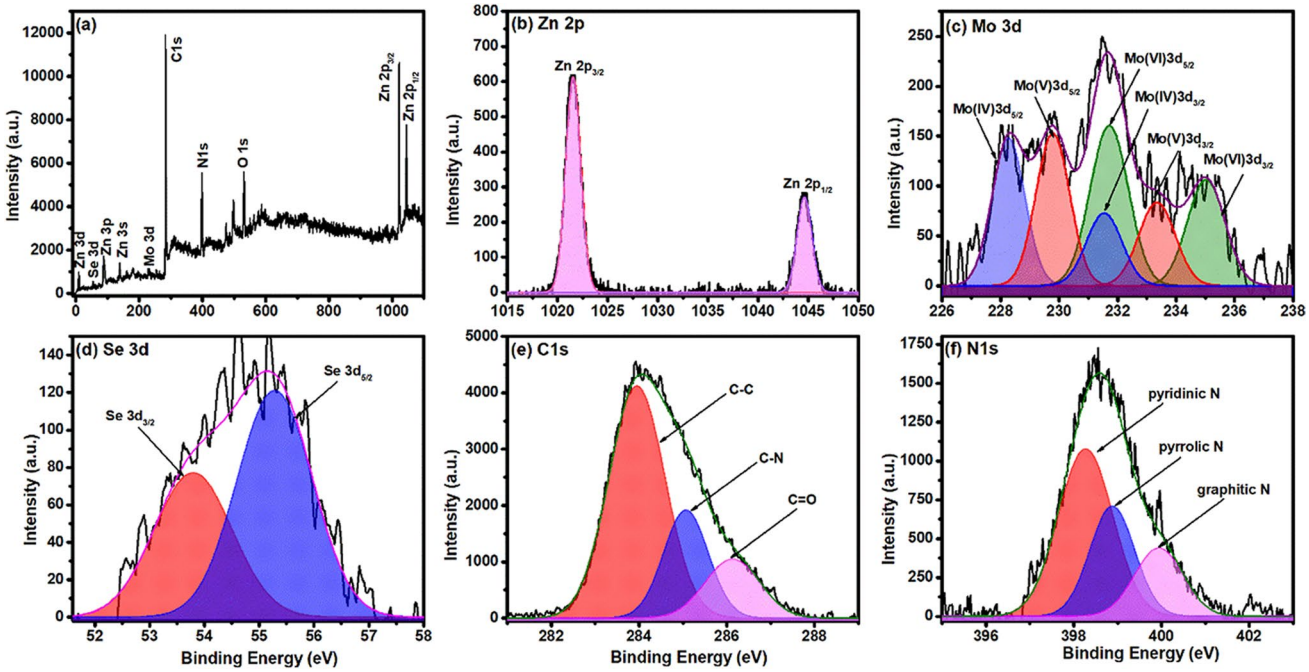

Fig. 5 (**a**) XPS survey spectra of ZM nanocomposite and high-resolution core spectra of (**b**) Zn 2p, (**c**) Mo 3d, (**d**) Se 3d, (**e**) N 1 s and (**f**) C1s

displayed in Fig. 5(d); the Se 3d core level demonstrates two peaks at 53.8 and 55.3 eV that can be attributed to Se $3d_{3/2}$ and Se $3d_{5/2}$, respectively, representing an oxidation state of − 2 for Se in $MoSe_2$ (Bi et al. 2015; Ge et al. 2018). The high-resolution N 1s core level spectrum in Fig. 5(e) can be deconvoluted into three prominent peaks at 398.3, 398.9 and 399.9 eV, which are attributed to the pyridinic, pyrrolic and graphitic nitrogen, respectively (Li et al. 2018). As shown in Fig. 5(f), the C 1s core level spectrum can be deconvoluted into three peaks centred at

283.9, 285.1 and 286.1 eV, corresponding to C–C, C–N and C–O bindings, respectively (Luanwuthi et al. 2015). It is observed that the binding energies of the Zn 2p, Mo 3d and Se 3d peaks in the ZM nanocomposite are shifted to lower binding energy by 1 eV, implying that $MoSe_2$ and ZIF-8 interact with each other (Chen et al. 2019). Thus, the above detailed material characterizations confirm the successful synthesis of the ZM nanocomposite.

Photocatalytic activity

The comparative photocatalytic degradation of metronidazole (MNZ) and tetracycline hydrochloride (TC) antibiotics and malachite green (MG) dye in aqueous solutions was performed using $MoSe_2$, ZIF-8 and ZM nanocomposites under light irradiation from a Xenon arc lamp (AM 1.5G solar illumination 100 mW/cm^2). For each photocatalytic degradation test, 20 mg of photocatalyst and 1 mg of the target pollutant were used in 100 mL of Milli-Q water. During light irradiation, 2 mL of the solution was taken out at a fixed interval for UV–Vis spectroscopy. The absorbance peaks for MNZ (318 nm), TC (357 nm) and MG (618 nm) were measured using UV–visible spectroscopy, and a decrease in intensity with irradiation time was measured (Huang et al. 2013; Medidi et al. 2018; Saghi and Mahanpoor 2017). The photocatalytic degradation efficiency (η)

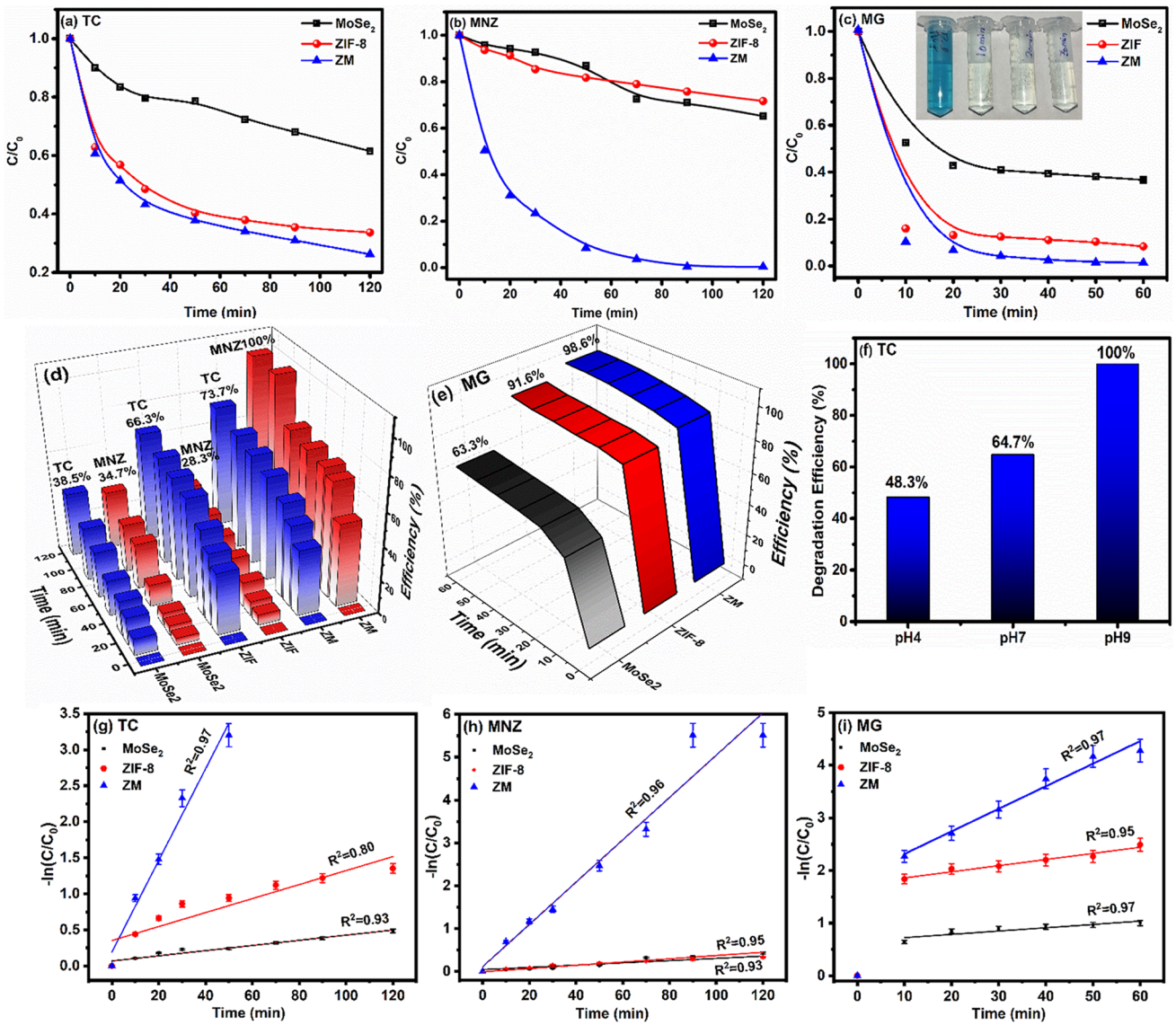

Fig. 6 Photocatalytic degradation performance of $MoSe_2$, ZIF-8 and ZM nanocomposite, C/C_0 plot for (**a**) TC (**b**) MNZ antibiotics and (**c**) MG dye; efficiency (η) vs time (min) plot for (**d**) TC, MNZ antibiotic and (**e**) MG dye; (**f**) degradation plot of TC under different pH conditions using ZM nanocomposite; First order kinetics plot of (**g**) TC, (**h**) MNZ and (**i**) MG

was calculated using $\eta = \left(1 - \frac{C}{C_0}\right)100\%$, where, C_0 and C represent degradation of pollutant before and after irradiation at time t, respectively.

The degradation and efficiency plots are shown in Fig. 6(a)–(e). The photocatalytic degradation efficiency for TC (Fig. 6(a)) by $MoSe_2$, ZIF-8 and ZM nanocomposites is 38.5%, 66.3% and 73.7%, respectively. The degradation of MNZ (Fig. 6(b)) by $MoSe_2$, ZIF-8 and ZM nanocomposites is 34.7%, 28.3% and 99.4%, respectively. The degradation of MG dye by $MoSe_2$, ZIF-8 and ZM nanocomposites is 63.3%, 91.6% and 99.4%, respectively. Malachite green dye was decolorized, as shown in the inset of Fig. 6(c). As observed from the results, the photocatalytic degradation efficiency of the ZM nanocomposite was enhanced as compared to pristine $MoSe_2$ and ZIF-8.

Photocatalytic properties

Effect of pH

The pH of the solution highly influences the photocatalytic degradation activity because it can affect both catalyst and pollutant. In this study, the photocatalytic degradation of TC by the ZM nanocomposite was studied under different pH conditions (acidic pH 4, basic pH 9 and neutral pH 7) as shown in Fig. 6(f). When the pH of the solution was 4, 7 and 9, the photocatalytic degradation efficiency of TC was 48%, 64.7% and 99.4%, respectively. The pH value of the solution affects not only the surface charge and physical–chemical properties of the pollutant and photocatalyst but also the generation of hydroxyl radicals. At lower pH, the primarily responsible oxidation species is photogenerated positive holes; however, at neutral pH or higher pH, it is hydroxyl radicals. According to the experiment, the pollutant degradation efficiency increases with the increasing pH of the solution.

Rate kinetics study

To further evaluate the photocatalytic process of the system, the kinetics of photocatalytic activity was studied using the pseudo-first-order kinetic equation that was used as follows:

$$-\ln\left(\frac{C_t}{C_o}\right) = kt \tag{2}$$

where k denotes the rate constant of the reaction.

The kinetic studies imply that degradation of TC, MNZ and MG by the ZM nanocomposite follows pseudo-first-order kinetics as shown in Fig. 6(g)–(i) with R^2 (linear correlation coefficient) values of 0.97, 0.96 and 0.97, respectively.

Table 1 Photodegradation efficiency, rate constant (k) and R^2 values of prepared photocatalysts

Pollutant	TC			MNZ			MG		
Photocatalyst	$MoSe_2$	ZIF-8	ZM	$MoSe_2$	ZIF-8	ZM	$MoSe_2$	ZIF-8	ZM
Efficiency (%)	38.5	66.3	100 (pH 9)	34.7	28.3	100	63.3	91.6	98.6
$k \times (10^{-3})$ (min^{-1})	3.5	9.7	63	2.6	3.8	49	6.2	11	42
R^2	0.80	0.93	0.97	0.93	0.95	0.96	0.97	0.95	0.97

The k (rate constant) linear correlation coefficient values for degradation of TC, MNZ and MG by ZM are 0.06 min^{-1}, 0.05 min^{-1} and 0.04 min^{-1}, respectively. The rate constant and linear coefficient values for the photocatalytic performance of $MoSe_2$, ZIF-8 and ZM nanocomposites are summarized in Table 1. The modified surface charge and improved charge transfer and separation in the ZM nanocomposite make it more favourable for photocatalytic activity.

Till date, several illustrations of semiconductor-MOF nanocomposites have been reported to show potential improvement in the photocatalytic activity; some of them are shown in Table 2 along with the results of the present study. These findings imply that ZIF-8 and $MoSe_2$ nanocomposites are promising photocatalysts for effective degradation of dye and antibiotics.

Surface charge

The surface charge of the photocatalyst plays an important role in the adsorption of the pollutant onto its

Table 2 The results of photocatalytic performance of ZIF-8, $MoSe_2$ and their nanocomposites reported in literature

Photocatalyst	Morphology	Pollutant	Efficiency (η)-light conditions	Reference
g-C_3N_4@ZIF-8	Rhombic dodecahedron	TC[1], RhB[2] and Cr(VI)[3]	TC (87.6%), Rh B (99.3%) and Cr(VI) (96.6%) in 60 min under the full spectrum irradiation	Yuan et al. (2021)
ZnCDs/ZnO@ZIF-8	Polyhedrons	TC[1]	85% in 200 min under visible-light illumination	Cheng et al. (2021)
Pt doped TiO_2-ZnO@ZIF-8	Polyhedral nanostructure	Phenol	86.9% in 24 h under UV light irradiation	Jing et al. (2022)
ZIF-8-derived ZnO@In_2O_3	Hollow microtubes	TC[1], MG[4], MB[5] and RhB[2]	TC (93.2%), MG (80.6%), MB (25.9%) and RhB (8.6%) in 200 min under AM 1.5G sunlight simulator	Li et al. (2021)
MoS_2-ZIF-8	Petal nanosheets	CIP[6] and TC[1]	CIP (93.2% in 180 min) and TC (75.6% in 180 min) -visible light irradiation	Chen et al. (2019)
Porous ZIF-8	-	MeB[7] and Flu[8]	MeB (99%) and Flu (25%) in 250 min under 450 W medium-pressure mercury vapor lamp	Soliman et al. (2022)
Ag/AgCl@ZIF-8 modified g-C_3N_4	Rhombic dodecahedron	Levofloxacin	87.3% in 60 min-visible light irradiations	Zhou et al. (2019)
CdS/MOF-derived porous carbon	Polyhedral crystals	Cephalexin	93.1% in 50 min-300 W Xe lamp	Yang et al. (2017)
ZIF-8@PTA@AuNP	Rhombic dodecahedron	TC[1]	~86%-UV light exposure	Beni et al. (2020)
Carbon nitride/porous zeolite	Globular tablet like	RhB[2], SuB[9], TC[1] and CIP[6]	98% (RhB), 96% (SuB), 95% (TC) and 92% (CIP)-light irradiation	Kumar et al. (2018)
MPg-C_3N_4-ZIF8	Spherical	TC[1]	74.8% in 180 min-visible light irradiations	Li et al. (2019a)
C_3N_4-ZIF8		TC[1]	96% in 60 min-sunlight	Panneri et al. (2017)
C-ZnS/$ZnMoO_4$ and C-ZnS/MoS_2 using ZIF8	Sphere like	TC[1] and RhB[2]	100% of TCH in 80 min and 100% of RhB in 120 min-300 W Xenon lamp	Cui et al. (2019)
ZIF-8	Nanoparticles	MB[5]	82.3%-visible light irradiation	Jing et al. (2014)
$MoSe_2$	Nanoflower	RhB[2]	99% within 5-min visible light irradiation	Jiang et al. (2017)
$MoSe_2$-PANI	Nanosheets	RhB[2] and CR[10]	99.1% CR in 120 min and 83.2% RhB in 150-min xenon arc lamp	Mittal et al. (2019)
$MoSe_2$-PPy	Nanoparticles	RhB[2] and CR[10]	98.6% CR in 15 min and 84.4% RhB in 15-min xenon arc lamp	Mittal and Khanuja (2021)
TiO_2@ZIF-8	Spherical	MB[5]	99.1% UV light irradiation for 180 min	Fu and Ren (2020)
TiO_2 NPs-ZIF8	Hexagonal	MB[5] and RhB[2]	93% of MB and 57% of RhB in 120-min UV–visible light irradiation	Chandra and Nath (2017)
$BiMoO_6$-ZIF8	Flower like structure	MB[5]	66.88% in 100-min 300-W Xe lamp with 420-nm cutoff filters	Xia et al. (2019)
$MoSe_2$@ZIF-8	Rhombic dodecahedron	TC[1], MNZ[11] and MG[4]	~100% of TC, MNZ in 120 min and 98.6% of MG in a 60-min Xenon arc lamp	Present study

[1]Tetracycline, [2]Rhodamine B, [3]Chromium hexavalent, [4]Malachite green, [5]Methylene blue, [6]Ciprofloxacin, [7]Methyl blue, [8]Fluorescein, [9]Sulforhodamine B, [10]Congo Red, [11]Metronidazole

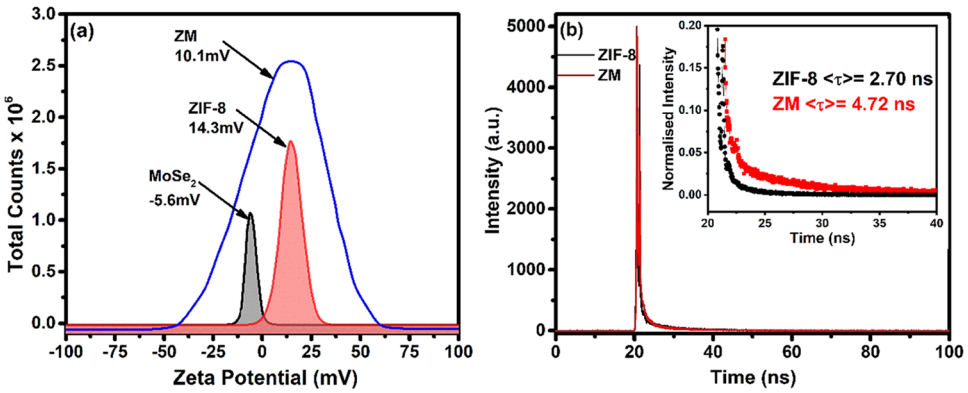

Fig. 7 (**a**) Zeta potential of $MoSe_2$, ZIF-8 and ZM nanocomposite and (**b**) TCSPC spectra of ZIF-8 and ZM nanocomposite upon excitation at 375 nm and emission at 425 nm, (inset) magnified image of TCSPC spectra

surface. As observed in Fig. 7(a), the surface charge of $MoSe_2$, ZIF-8 and ZM nanocomposite is found to be − 5.6, 14.3 and 10.1 mV, respectively. The surface charge of TC at 4 < pH < 7 is positive whereas at 9 < pH < 12 is negative (Li et al. 2019a). The surface charge of MNZ is neutral in the range of 4 < pH < 10 so it is not affected by the pH conditions (Carrales-Alvarado et al. 2014). As observed in Fig. 6(f), ZM has high photocatalytic degradation efficiency for TC at pH 9 because of the competitive electrostatic attraction between the active species of TC (TC^{2-}) and the positive surface of the ZM nanocomposite. However, when pH is 4 or 7, the dominant species of TC are TCH_2 and TCH^- and the adsorption capacity of ZM decreases because of the electrostatic repulsion (Li et al. 2019a). The higher degradation efficiency at basic conditions is in agreement with the zeta potential results.

Photogenerated charge carrier lifetime study

The photogenerated charge carrier dynamics have been studied with the time-correlated single-photon counting system (TCSPC) for ZIF-8 and ZM nanocomposites, and the decay spectra are fitted with exponential function as shown in Fig. 7(b) (Mittal and Khanuja 2020b). The magnified portion of the spectra is as shown in the inset of Fig. 7(b). The average lifetime of photogenerated charge carriers in ZIF-8 and ZM nanocomposites were obtained to be 2.70 ns and

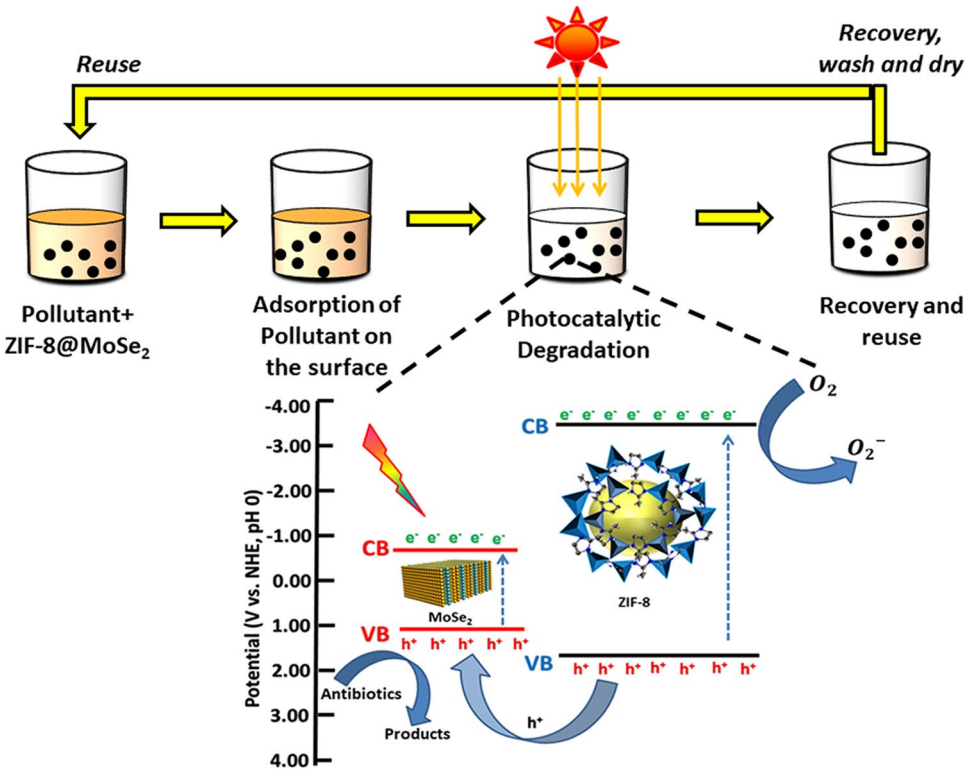

Fig. 8 Schematic illustration of photocatalytic mechanism, reusability and charge transfer in the ZM nanocomposite under visible light irradiation

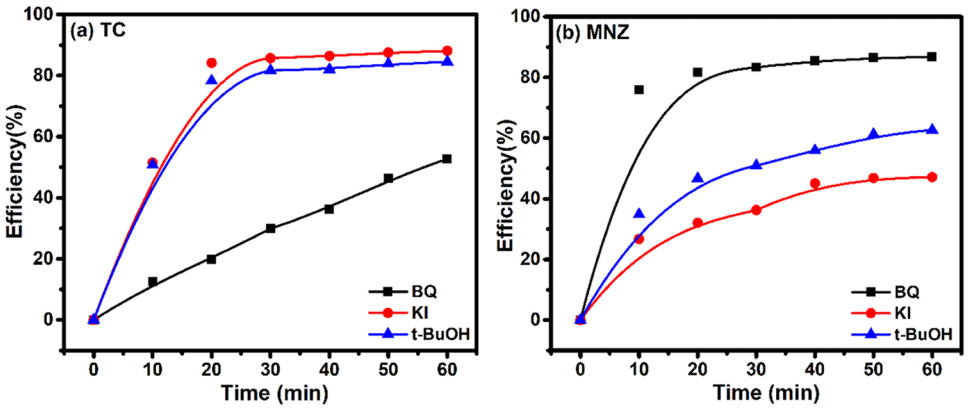

Fig. 9 Photocatalytic degradation efficiency of ZM nanocomposite in the presence of para-benzoquinone (BQ), potassium iodide (KI) and tert-butyl alcohol (t-BuOH) for (**a**) TC and (**b**) MNZ

4.72 ns, respectively. The TCSPC results confirm that the construction of ZM nanocomposite is advantageous for efficient charge-carrier separation, which results in high photocatalytic activity for the nanocomposite.

Photocatalysis mechanism

The photocatalytic degradation mechanism of the ZM nanocomposite was proposed, and the schematic is as shown in Fig. 8. The heterojunction created by ZIF-8 and $MoSe_2$ is advantageous in enhancing photocatalytic activity by improving the photogenerated charge carrier generation, transfer and separation. $MoSe_2$ and ZIF-8 could be excited by the light irradiation of energy larger than that of their forbidden band and photoinduced electrons transferred from the valence band to the conduction band in both ZIF-8 and $MoSe_2$. The photoinduced holes can be transferred from the VB of ZIF-8 (1.68 V) to the VB of $MoSe_2$ (1.2 V), which helps in reducing the recombination rate (Mittal and Khanuja 2021; Wang et al. 2020b). However, due to the CB position of ZIF-8 (−3.41 V), the photogenerated electrons cannot move to the CB of $MoSe_2$ (−0.21 V) (Mittal and Khanuja 2021; Wang et al. 2020b). The electrons in CB can react with the dissolved O_2 to generate superoxide radicals ($O_2^{\bullet-}$) and holes in the VB react with water to form hydroxyl radicals ($OH^{\bullet}$). These radicals can react with the adsorbed pollutant and decompose it into simple and non-toxic molecules.

Scavenger test

To investigate the generation of active species and their role in the photocatalytic degradation process, tetra-butyl alcohol (t-BuOH), potassium iodide (KI) and para-benzoquinone (BQ) were used as $OH^{\bullet}$, $OH^{\bullet}$ andh^{+}, and $O_2^{\bullet-}$ quenchers, respectively (Mittal and Khanuja 2020c). The photocatalysis was performed in the presence of 20 mg of the ZM nanocomposite in 100 mL of each TC and MNZ solution (1 mg/100 mL) and 1 mM of each scavenger under light irradiation for 60 min, and efficiency results are shown in Fig. 9(a) and (b), respectively. The photodegradation efficiency of ZM for TC and MNZ was ~ 100% without any scavenger in the solution, and the photocatalytic degradation performance was significantly reduced with the addition of quenchers, and the degradation efficiency for TC was 52.7% with addition of BQ, 84.5% with t-BuOH and 88.1% when KI was added. It can be concluded that the superoxide radicals are the main free radicals that are responsible for the degradation of TC (Qiang et al. 2019). In the scavenger test for the degradation of MNZ, the final degradation rate was 42.1% with addition of KI, 62.6% with t-BuOH and 86.7% when BQ was added. It can be concluded that the holes and hydroxyl radicals are mainly responsible for the degradation of MNZ (Ahmaruzzaman et al. 2019).

Possible photocatalytic degradation pathway of TC by LC–MS

The intermediate products generated during photocatalytic degradation of TC were investigated by LC–MS using the solution which were collected during photocatalytic reaction at 10 min and 120 min. Figure 10(a) and (b) show the chromatographs at 10 and 120 min, respectively. The chromatograph in Fig. 10(a) shows that the TC (m/z = 445) degraded into the product with m/z value of 460 due to the hydroxylation of aromatic ring (Jeong et al. 2010; Li et al. 2019c; Luo et al. 2020). Further, the simultaneously demethylation and oxidation of the TC resulted in the formation of a product with m/z value of 432 (Wang et al. 2018). The chromatograph shows that TC was further oxidized by radicals, resulting in the formation of ketone and a methyl group, forming a new product after 120 min with m/z values of 433 and 415 (Zhang et al. 2020). The stepwise attack of reactive oxygen species resulted in the simultaneous destruction of the 4-ring structure by deamination, and dihydroxylation resulted into products with m/z values of 244, 222 and 175. The resulting product is further degraded into the product with m/z value of

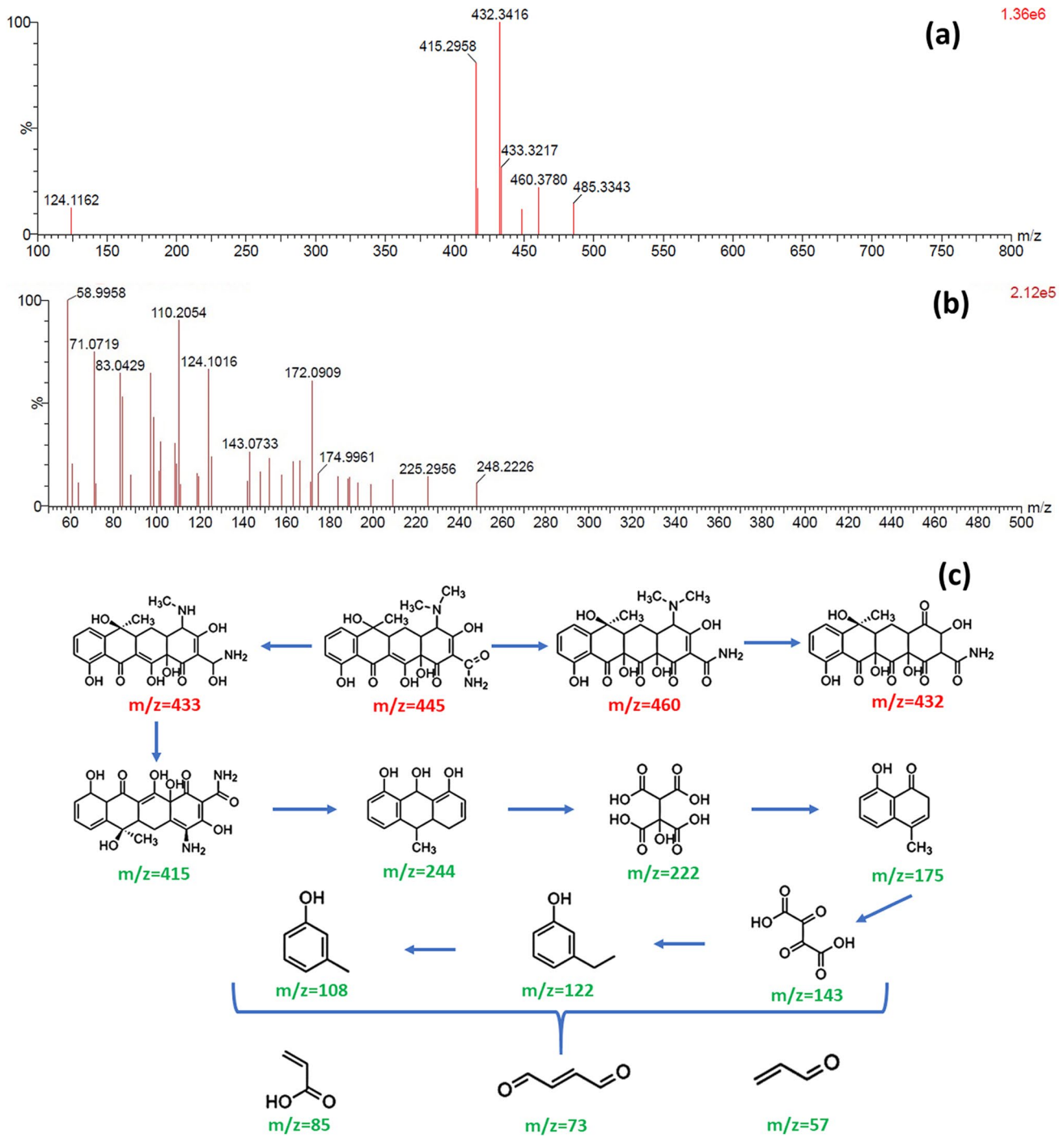

Fig. 10 LC–MS spectrum of degraded solution of TC at (**a**) 10 min, (**b**) 120 min and (**c**) possible photocatalytic degradation pathway for TC

143 via adding hydroxyl groups, which in turn leads to the generation of product with m/z value of 122 via dihydroxylation (Niu et al. 2013). The simpler ring-opened products, with m/z values of 85, 73 and 57, are the final products formed after the photocatalytic degradation for 120 min (Li et al. 2019c). The degradation pathway was proposed using these identified intermediate products, and the structural identification and m/z of these intermediate are shown in Fig. 10(c). The intermediate products of m/z 460, 433 and 432 (labelled with red colour in Fig. 10(c)) are as toxic as TC, but the finally degraded products (labelled with green colour in Fig. 10(c)) are not harmful

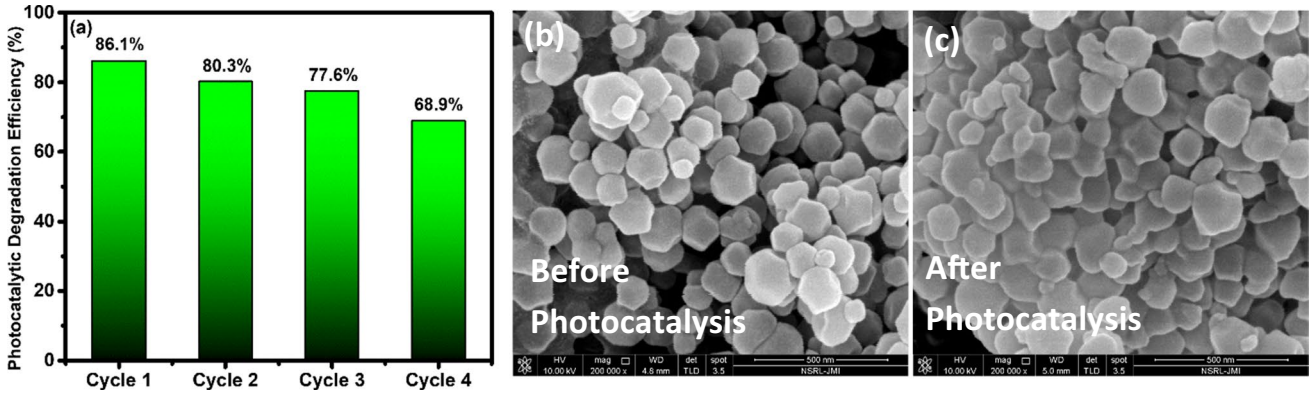

Fig. 11 Reusability and regeneration of the ZM nanocomposite: (**a**) 4 cycles of the photocatalytic degradation of TC; FESEM image of the ZM nanocomposite (**b**) before photocatalysis and (**c**) after 4 cycles of photocatalysis

to the aquatic life (Wang et al. 2018). After 120 min of photocatalytic reaction, 99.4% of TC was degraded using the ZM nanocomposite. Hence, the ZM nanocomposite exhibited a desirable degradation efficiency and a promising application potential for antibiotic waste–contaminated water treatment.

Reusability of the $MoSe_2$@ZIF-8 nanocomposite

To determine the reusability and regeneration ability of the ZM nanocomposite, four cycles of the photocatalytic degradation of TC were performed under light irradiation using 50 mg of ZM for the degradation of TC with a concentration of 10 mg L^{-1}. After each cycle of the photocatalytic degradation, the ZM was extracted from the degradation solution by filtration and washed by Milli-Q water, followed by drying at 60 ℃ for 4 h. The ZM nanocomposite showed good photocatalytic degradation efficiencies, as shown in Fig. 11(a). The regeneration efficiency of the nanocomposite as calculated using Eq. (3) is 93.2%, 96.6% and 88.7% in 2, 3 and 4 cycles, respectively.

$$\text{Regeneration efficiency } (\%) = \frac{\text{Degradation efficiency in } n\text{th cycle}}{\text{Degradation efficiency in } (n-1)\text{th cycle}} \times 100 \quad (3)$$

Moreover, the FESEM images of the as-prepared ZM nanocomposite and after 4 cycles of photocatalytic degradation are shown in Fig. 11(b) and (c), respectively. There is no visible change in the morphology of the catalyst. This indicates that the ZM nanocomposite is a suitable and potential candidate for practical applications as a photocatalyst.

Conclusion

This study provided a cost-effective and potential photocatalytic material, which has the capability to treat water, contaminated with antibiotic waste used for COVID-19. The superior degradation efficiencies were achieved for tetracycline hydrochloride, metronidazole antibiotics and malachite green dye. As observed from the results, the photocatalytic degradation efficiency of the ZM nanocomposite was enhanced as compared to pristine $MoSe_2$ and ZIF-8 and the enhancement could be attributed to the competitive absorption on the surface (as described through zeta potential) of the nanocomposite and improved photogenerated charge transfer and separation efficiency (as explained through TCSPC results) resulting from the heterojunction between ZIF-8 and $MoSe_2$. pH = 9 is optimal from the degradation rate of the tetracycline hydrochloride antibiotic. In the photocatalytic degradation of antibiotics, the main active species for degrading tetracycline hydrochloride is superoxide radicals, while the main active species for the degradation of metronidazole are holes and hydroxyl radicals. The finally degraded products of the antibiotic (TC) were not harmful to the aquatic organisms (as confirmed through LC–MS). The photocatalyst retained good regeneration ability after four consecutive cycles, thereby confirming the reusability and regeneration ability of the ZM nanocomposite.

Acknowledgements The authors would like to acknowledge the MRC, MNIT Jaipur and CIF, JMI, New Delhi.

Author contribution All authors contributed to the study conception and design. Material preparation, data collection and analysis were performed by Honey Mittal, Aruna Ivaturi and Manika Khanuja. All authors read and approved the final manuscript.

Funding This work is financially supported by the Department of Science and Technology, India (DST/NM/NB/2018/203(G)(JMI)), Science and Engineering Research Board, India (SERB, ECR/2017/001222), and Scottish Funding Council (SFC) Global Challenge Research Fund (GCRF) David Livingston Fellowship Project 2019–20.

Data availability No datasets were generated or analysed during the current study.

Declarations

Ethical approval We consciously assure that the manuscript is our own original work, which has not been previously published elsewhere.

Consent to participate All authors have been personally and actively involved in substantial work leading to the paper, and will take public responsibility for its content.

Consent for publication We have seen a version of the manuscript to be submitted/published (including any pictures) and we hereby give our consent for publication in the Environmental Science and Pollution Research.

Competing interests The authors declare no competing interests.

References

Adams C, Wang Y, Loftin K, Meyer M (2002) Removal of antibiotics from surface and distilled water in conventional water treatment processes. J Environ Eng 128:253–260

Ahmaruzzaman M, Mohanta D, Nath A (2019) Environmentally benign fabrication of SnO_2-CNT nanohybrids and their multifunctional efficiency as an adsorbent, catalyst and antimicrobial agent for water decontamination. Sci Rep 9:12935

Ashraf W, Bansal S, Singh V, Barman S, Khanuja M (2020) BiOCl/WS_2 hybrid nanosheet (2D/2D) heterojunctions for visible-light-driven photocatalytic degradation of organic/inorganic water pollutants. RSC Adv 10:25073–25088

Barhoumi N, Oturan N, Ammar S, Gadri A, Oturan MA, Brillas E (2017) Enhanced degradation of the antibiotic tetracycline by heterogeneous electro-Fenton with pyrite catalysis. Environ Chem Lett 15:689–693

Beni FA, Gholami A, Ayati A, Shahrak MN, Sillanpää M (2020) UV-switchable phosphotungstic acid sandwiched between ZIF-8 and Au nanoparticles to improve simultaneous adsorption and UV light photocatalysis toward tetracycline degradation. Microporous Mesoporous Mater 303:110275

Bi E, Chen H, Yang X, Ye F, Yin M, Han L (2015) Fullerene-structured $MoSe_2$ hollow spheres anchored on highly nitrogen-doped graphene as a conductive catalyst for photovoltaic applications. Sci Rep 5:13214

Carrales-Alvarado D, Ocampo-Pérez R, Leyva-Ramos R, Rivera-Utrilla J (2014) Removal of the antibiotic metronidazole by adsorption on various carbon materials from aqueous phase. J Colloid Interface Sci 436:276–285

Chandra R, Nath M (2017) Multi-core-shell TiO_2NPs@ZIF-8 composite for enhanced photocatalytic degradation and adsorption of methylene blue and rhodamine-B. ChemistrySelect 2:7711–7722

Chen W-Q, Li L-Y, Li L, Qiu W-H, Tang L, Xu L, Xu K-J, Wu M-H (2019) MoS_2/ZIF-8 hybrid materials for environmental catalysis: solar-driven antibiotic-degradation engineering. Engineering 5:755–767

Chen Z, Guo J, Jiang Y, Shao Y (2021) High concentration and high dose of disinfectants and antibiotics used during the COVID-19 pandemic threaten human health. Environ Sci Eur 33:11. https://doi.org/10.1186/s12302-021-00456-4

Cheng Y, Wang X, Mei Y, Wang D, Ji C (2021) ZnCDs/ZnO@ZIF-8 Zeolite composites for the photocatalytic degradation of tetracycline. Catalysts 11:934

Chin M, Cisneros C, Araiza SM, Vargas KM, Ishihara KM, Tian F (2018) Rhodamine B degradation by nanosized zeolitic imidazolate framework-8 (ZIF-8). RSC Adv 8:26987–26997

Cui Y-W, Zhang H-H, Yu S-Y (2019) Constructing ZIF-8 derived C-ZnS/$ZnMoO_4$@MoS_2 and C–ZnS/MoS_2 nanocomposites using a simple one-pot strategy to enhance photocatalytic degradation activity. RSC Adv 9:35189–35196

Daghrir R, Drogui P (2013) Tetracycline antibiotics in the environment: a review. Environ Chem Lett 11:209–227

Dharmaraj S, Ashokkumar V, Pandiyan R, Munawaroh HSH, Chew KW, Chen W-H, Ngamcharussrivichai C (2021) Pyrolysis: An effective technique for degradation of COVID-19 medical wastes. Chemosphere 275:130092

Fu N, Ren X-C (2020) Synthesis of double-shell hollow TiO_2@ZIF-8 nanoparticles with enhanced photocatalytic activities. Front Chem 8:578847

Ge P, Hou H, Banks CE, Foster CW, Li S, Zhang Y, He J, Zhang C, Ji X (2018) Binding $MoSe_2$ with carbon constrained in carbonous nanosphere towards high-capacity and ultrafast Li/Na-ion storage. Energy Storage Mater 12:310–323

Gharebaghi R, Heidary F, Moradi M, Parvizi M (2020) Metronidazole; a potential novel addition to the COVID-19 treatment regimen. Arch Acad Emerg Med 8:e40

Gironi LC, Damiani G, Zavattaro E, Pacifico A, Santus P, Pigatto PDM, Cremona O, Savoia P (2020) Tetracyclines in COVID-19 patients quarantined at home: literature evidence supporting Real-World Data from a Multicenter Observational Study Targeting Inflammatory & Infectious Dermatoses. Dermatol Ther 34:e14694

Harpeness R, Gedanken A, Weiss A, Slifkin M (2003) Microwave-assisted synthesis of nanosized $MoSe_2$. J Mater Chem 13:2603–2606

Huang Q, Li B, Yang S, Ma P, Wang Z (2013) Preparation and cyclodextrin solubilization of the antibacterial agent benzoyl metronidazole. Sci World J 2013:306476

Jeong J, Song W, Cooper WJ, Jung J, Greaves J (2010) Degradation of tetracycline antibiotics: mechanisms and kinetic studies for advanced oxidation/reduction processes. Chemosphere 78:533–540

Jia G, Liu L, Zhang L, Zhang D, Wang Y, Cui X, Zheng W (2018) 1D alignment of ZnO@ZIF-8/67 nanorod arrays for visible-light-driven photoelectrochemical water splitting. Appl Surf Sci 448:254–260

Jiang Q, Lu Y, Huang Z, Hu J (2017) Facile solvent-thermal synthesis of ultrathin $MoSe_2$ nanosheets for hydrogen evolution and organic dyes adsorption. Appl Surf Sci 402:277–285

Jing H-P, Wang C-C, Zhang Y-W, Wang P, Li R (2014) Photocatalytic degradation of methylene blue in ZIF-8. RSC Adv 4:54454–54462

Jing Y, Yin H, Li C, Chen J, Wu S, Liu H, Xie L, Lei Q, Sun M, Yu S (2022) Fabrication of Pt doped TiO_2–ZnO@ ZIF-8 core@shell photocatalyst with enhanced activity for phenol degradation. Environ Res 203:111819

Kaur H, Mohanta GC, Gupta V, Kukkar D, Tyagi S (2017) Synthesis and characterization of ZIF-8 nanoparticles for controlled release of 6-mercaptopurine drug. J Drug Deliv Sci Technol 41:106–112

Kumar A, Samanta S, Srivastava R (2018) Systematic investigation for the photocatalytic applications of carbon nitride/porous zeolite heterojunction. ACS Omega 3:17261–17275

Kumar A, Singh S, Khanuja M (2020) A comparative photocatalytic study of pure and acid-etched template free graphitic C_3N_4 on different dyes: an investigation on the influence of surface modifications. Mater Chem Phys 243:122402

Kumar A, Mittal H, Nagar R, Khanuja M (2022) The synergistic effect of acid-etched gC_3N_4 nanosheets and polyaniline nanofibers for the adsorption and photocatalytic degradation of textile dyes: a study of charge transfer mechanism and intermediate products. Mater Adv 3:5325–533. https://doi.org/10.1039/D1MA01218E

Li Y, Cai X, Chen S, Zhang H, Zhang KH, Hong J, Chen B, Kuo D-H, Wang W (2018) Highly dispersed metal carbide on ZIF-derived pyridinic-N-doped carbon for CO_2 enrichment and selective hydrogenation. ChemSusChem 11:1040–1047

Li D, Liu H, Niu C, Yuan J, Xu F (2019a) Mpg-C_3N_4-ZIF-8 composites for the degradation of tetracycline hydrochloride using visible light. Water Sci Technol 80:2206–2217

Li N, Zhou L, Jin X, Owens G, Chen Z (2019b) Simultaneous removal of tetracycline and oxytetracycline antibiotics from wastewater using a ZIF-8 metal organic-framework. J Hazard Mater 366:563–572

Li Z, Guo C, Lyu J, Hu Z, Ge M (2019c) Tetracycline degradation by persulfate activated with magnetic Cu/$CuFe_2O_4$ composite: efficiency, stability, mechanism and degradation pathway. J Hazard Mater 373:85–96

Li Z, Sun Y, Yang Y, Han Y, Wang T, Chen J, Tsang DC (2020) Comparing biochar-and bentonite-supported Fe-based catalysts for selective degradation of antibiotics: mechanisms and pathway. Environ Res 183:109156

Li J, Liu L, Liang Q, Zhou M, Yao C, Xu S, Li Z (2021) Core-shell ZIF-8@MIL-68 (In) derived ZnO nanoparticles-embedded In_2O_3 hollow tubular with oxygen vacancy for photocatalytic degradation of antibiotic pollutant. J Hazard Mater 414:125395

Liu Z, Zhang Y, Zhao H, Li N, Du Y (2017) Constructing monodispersed $MoSe_2$ anchored on graphene: a superior nanomaterial for sodium storage. Sci China Mater 60:167–177

Luanwuthi S, Krittayavathananon A, Srimuk P, Sawangphruk M (2015) In situ synthesis of permselective zeolitic imidazolate framework-8/graphene oxide composites: rotating disk electrode and Langmuir adsorption isotherm. RSC Adv 5:46617–46623

Luo T, Feng H, Tang L, Lu Y, Tang W, Chen S, Yu J, Xie Q, Ouyang X, Chen Z (2020) Efficient degradation of tetracycline by heterogeneous electro-Fenton process using Cu-doped Fe@Fe_2O_3: Mechanism and degradation pathway. Chem Eng J 382:122970

Medidi S, Markapurapu S, Kotupalli MR, Chinnam RKR, Susarla VM, Gandham HB, Sanasi PD (2018) Visible light photocatalytic degradation of methylene blue and malachite green dyes with $CuWO_4$-GO nano composite. Mod Res Catal 7:17–34

Mittal H, Khanuja M (2020a) Nanosheets-and nanourchins-like nanostructures of $MoSe_2$ for photocatalytic water purification: kinetics and reusability study. Environ Sci Pollut Res 27:23477–23489

Mittal H, Khanuja M (2020b) Interfacial charge carrier dynamics of the $MoSe_2$-conducting polymer ($MoSe_2$-PANI) heterojunction. Mater Today: Proc 28:314–316

Mittal H, Khanuja M (2020c) Optimization of $MoSe_2$ nanostructure by surface modification using conducting polymer for degradation of cationic and anionic dye: Photocatalysis mechanism, reaction kinetics and intermediate product study. Dyes Pigm 175:108109

Mittal H, Khanuja M (2021) Hydrothermal in-situ synthesis of $MoSe_2$-polypyrrole nanocomposite for efficient photocatalytic degradation of dyes under dark and visible light irradiation. Sep Purif Technol 254:117508

Mittal H, Kumar A, Khanuja M (2019) In-situ oxidative polymerization of aniline on hydrothermally synthesized $MoSe_2$ for enhanced photocatalytic degradation of organic dyes. J Saudi Chem Soc 23:836–845

Niu J, Ding S, Zhang L, Zhao J, Feng C (2013) Visible-light-mediated Sr-Bi_2O_3 photocatalysis of tetracycline: kinetics, mechanisms and toxicity assessment. Chemosphere 93:1–8. https://doi.org/10.1016/j.chemosphere.2013.04.043

Panneri S, Thomas M, Ganguly P, Nair BN, Mohamed AP, Warrier K, Hareesh U (2017) C_3N_4 anchored ZIF 8 composites: photoregenerable, high capacity sorbents as adsorptive photocatalysts for the effective removal of tetracycline from water. Catal Sci Technol 7:2118–2128

Peng H-J, Zheng P-Q, Chao H-Y, Jiang L, Qiao Z-P (2020) CdSe/ZIF-8-x: synthesis and photocatalytic CO_2 reduction performance. RSC Adv 10:551–555

Qiang N, Shi T, Liu T (2019) In-depth study of the key factors affecting the degradation of antibiotics by carbon nitride and its modified photocatalytic materials, IOP Conference Series: Earth and Environmental Science. IOP Publishing 3:032051

Qin K, Zhao Q, Yu H, Xia X, Li J, He S, Wei L, An T (2021) A review of bismuth-based photocatalysts for antibiotic degradation: insight into the photocatalytic degradation performance, pathways and relevant mechanisms. Environ Res 199:111360

Qiu J, Zhang X, Feng Y, Zhang X, Wang H, Yao J (2018) Modified metal-organic frameworks as photocatalysts. Appl Catal B 231:317–342

Saghi M, Mahanpoor K (2017) Photocatalytic degradation of tetracycline aqueous solutions by nanospherical α-Fe_2O_3 supported on 12-tungstosilicic acid as catalyst: Using full factorial experimental design. Int J Ind Chem 8:297–313

Shinde P, Sharma V, Punde A, Waghmare A, Vairale P, Hase Y, Pandharkar S, Bhorde A, Aher R, Nair S (2021) 2D alignment of zinc oxide@ ZIF8 nanocrystals for photoelectrochemical water splitting. New J Chem 45:3498–3507

Si Y-H, Li Y-Y, Xia Y, Shang S-K, Xiong X-B, Zeng X-R, Zhou J (2018) Fabrication of novel ZIF-8@$BiVO_4$ composite with enhanced photocatalytic performance. Curr Comput-Aided Drug Des 8:432

Siddiqui I, Mittal H, Kohli VK, Gautam P, Ali M, Khanuja M (2018) Hydrothermally synthesized micron sized, broom-shaped $MoSe_2$ nanostructures for superior photocatalytic water purification. Mater Res Express 5:125020

Sodhi M, Etminan M (2020) Therapeutic potential for tetracyclines in the treatment of COVID-19. Pharmacotherapy J Hum Pharmacol Drug Ther 40: 487–488

Soliman AI, Abdel-Wahab A-MA, Abdelhamid HN (2022) Hierarchical porous zeolitic imidazolate frameworks (ZIF-8) and ZnO@N-doped carbon for selective adsorption and photocatalytic degradation of organic pollutants. RSC Adv 12:7075–7084

Stackelberg PE, Gibs J, Furlong ET, Meyer MT, Zaugg SD, Lippincott RL (2007) Efficiency of conventional drinking-water-treatment processes in removal of pharmaceuticals and other organic compounds. Sci Total Environ 377:255–272

Tsai W-T (2021) Analysis of medical waste management and impact analysis of COVID-19 on its generation in Taiwan. Waste Manag Res 39: 27–33, 0734242X21996803

Ulu A (2020) Metal–organic frameworks (MOFs): a novel support platform for ASNase immobilization. J Mater Sci 55:6130–6144

Wang J, Zhi D, Zhou H, He X, Zhang D (2018) Evaluating tetracycline degradation pathway and intermediate toxicity during the electrochemical oxidation over a Ti/Ti_4O_7 anode. Water Res 137:324–334

Wang F, Zhang Y, Ming H, Wang L, Zhao Z, Wang Y, Liang J, Qin Y (2020a) Degradation of the ciprofloxacin antibiotic by photo-Fenton reaction using a Nafion/iron membrane: role of hydroxyl radicals. Environ Chem Lett 18:1745–1752

Wang T, Wang Y, Sun M, Hanif A, Wu H, Gu Q, Ok YS, Tsang DC, Li J, Yu J (2020b) Thermally treated zeolitic imidazolate framework-8 (ZIF-8) for visible light photocatalytic degradation of gaseous formaldehyde. Chem Sci 11:6670–6681

Wu C, Liu Q, Chen R, Liu J, Zhang H, Li R, Takahashi K, Liu P, Wang J (2017) Fabrication of ZIF-8@SiO_2 micro/nano hierarchical superhydrophobic surface on AZ31 magnesium alloy with impressive corrosion resistance and abrasion resistance. ACS Appl Mater Interfaces 9:11106–11115

Xia Y, Shang S-k, Zeng X-r, Zhou J, Li Y-y (2019) A novel Bi_2MoO_6/ZIF-8 composite for enhanced visible light photocatalytic activity. Nanomaterials 9:545

Yang C, Cheng J, Chen Y, Hu Y (2017) CdS nanoparticles immobilized on porous carbon polyhedrons derived from a metal-organic framework with enhanced visible light photocatalytic activity for antibiotic degradation. Appl Surf Sci 420:252–259

Yuan X, Qu S, Huang X, Xue X, Yuan C, Wang S, Wei L, Cai P (2021) Design of core-shelled g-C_3N_4@ZIF-8 photocatalyst with enhanced tetracycline adsorption for boosting photocatalytic degradation. Chem Eng J 416:129148

Zhang Q, Jiang L, Wang J, Zhu Y, Pu Y, Dai W (2020) Photocatalytic degradation of tetracycline antibiotics using three-dimensional network structure perylene diimide supramolecular organic photocatalyst under visible-light irradiation. Appl Catal B 277:119122

Zhou J, Liu W, Cai W (2019) The synergistic effect of Ag/AgCl@ZIF-8 modified g-C_3N_4 composite and peroxymonosulfate for the enhanced visible-light photocatalytic degradation of levofloxacin. Sci Total Environ 696:133962